Eur. Phys. J. E (2017) **40**: 78
DOI 10.1140/epje/i2017-11568-6

THE EUROPEAN PHYSICAL JOURNAL E

Regular Article

Studies on electrostatic interactions within model nano-confined aqueous environments of different chemical nature

Joan Manuel Montes de Oca[1], Cintia A. Menéndez[1], Sebastián R. Accordino[1], David C. Malaspina[2], and Gustavo A. Appignanesi[1,a]

[1] INQUISUR, Departamento de Química, Universidad Nacional del Sur (UNS)-CONICET, Avenida Alem 1253, 8000 Bahía Blanca, Argentina
[2] Biomedical Engineering Department, Northwestern University, 2145 Sheridan Road, Evanston, IL, 60208, USA

Received 1 September 2017
Published online: 20 September 2017 –

Abstract. We study the potential of mean force for pairs of parallel flat surfaces with attractive electrostatic interactions by employing model systems functionalized with different charged, hydrophobic and hydrophilic groups. We study the way in which the local environment (hydrophobic or hydrophilic moieties) modulates the interaction between the attractive charged groups on the plates by removing or attracting nearby water and thus screening or not the electrostatic interaction. To explicitly account for the role of the solvent and the local hydrophobicity, we also perform studies *in vacuo*. Additionally, the results are compared to that for non-charged plates in order to single out and rationalize the non-additivity of the different non-covalent interactions. Our simulations demonstrate that the presence of neighboring hydrophobic groups promote water removal in the vicinity of the charged groups, thus enhancing charge attraction upon self-assembly. This role of the local hydrophobicity modulating electrostatic interactions is consistent with recent qualitative descriptions in the protein binding context.

1 Introduction

A full comprehension of hydrophobicity at the nanoscale encompassing the way in which non-covalent interactions are modulated under nano-confinement conditions is still lacking. Such knowledge is demanded not only in order to rationalize self-assembly processes in various contexts, ranging from biology to materials design, but also to allow for rational design efforts in such fields [1–9]. In self-assembly processes, water acts as a mediator between complex surfaces that interact mainly between non-covalent interactions within an environment characterized by nanometric dimensions [4, 7, 10–16]. Indeed, the self-assembly of large (nanoscale) hydrophobic surfaces depends on the occurrence of a dewetting or drying transition at certain critical separation below which the liquid becomes thermodynamically unstable [7, 17–19]. Additionally, it has been shown that hydrophobicity depends non-trivially on the patterning or arrangement of hydrophobic and hydrophilic sites on the interacting surfaces [7, 10, 19–21]. In fact, calculations for parallel plates with identical compositions (equal number of charged and hydrophobic sites) but arranged in different patterns produced very different potential of mean force profiles. This speaks of a highly cooperative nature of the hydrophobic effect and, thus, a clear non-additivity of the corresponding non-covalent interactions [19]. It would be thus of great relevance to fully rationalize such non-additive behavior and to determine possible design elements of interest in self-assembly in order to aid rational design endeavors. Our present work attempts to make a step in this way.

The above-described behavior is consistent with a scenario for protein binding that has explained protein-protein complexes and that has yielded successful drug design efforts [22, 23]. Such approach is based precisely on the recognition of the context dependence of non-covalent interactions of electrostatic nature, like protein backbone hydrogen bonds. Such interactions require a proper protection (wrapping [22, 23]) from water attack by means of hydrophobic groups in order to be stable in solution and, thus, the existence of packing defects (dehydrons [22, 23]) at the protein surface become essential for binding [22–29]. Additionally, the O-Ring theory of protein binding [30, 31] also implies the fact that (usually flat) protein binding hotspots are made up of a small group of residues that mainly contribute to the binding energy (as determined, for instance, by alanine scanning experiments), which are located at the centre of the interface. Such residues are surrounded by a group of energetically non-important residues, whose role is precisely to occlude solvent form the interaction region. Thus, these

[a] e-mail: appignan@criba.edu.ar

rim-like arranged residues generate suitable effective dielectric and solvation conditions for the central interacting residues. A lower effective dielectric, for instance, would increase the strength of electrostatic interactions in hotspots.

Within this context, the aim of our present work is to rationalize the non-additive nature of electrostatic non-covalent interactions during (hydrophobic) collapse in model self-assembly processes. Thus, we shall study simple systems represented by flat surfaces in which a reactive charged site is placed within different local environments. Potential of mean force calculations will then be performed for pairs of attractive surfaces. Our results will demonstrate that a proper modulation by means of hydrophobic groups of the local context of electrostatic interactions clearly enhances the interaction strength upon self-assembly.

2 Methodology

We studied the thermodynamics of the binding process of two simple model surfaces consistent in parallel plates, both in water and *in vacuo*. Each plate was built functionalizing a scaffold diamond slab to give an arrangement of hexagons very similar in geometry to the hexagonal self-assembled monolayer over the $(1, 1, 1)$ face of gold. The first set of systems was composed of oppositely charged slabs with a variety of surrounding groups of different hydrophobicity (from hydrophilic to hydrophobic as shown in fig. 1).

All the systems were hydrated using TIP3P water model in a rectangular box of roughly $5 \times 7 \times 5$ nm. The molecular dynamics simulations were conducted using GROMACS package version 5.1.1 [32] with AMBER99 force field [33]. All the bonds were constrained using the LINCS algorithm, the long range electrostatic forces were evaluated with the PME method. We used a modified Berendsen thermostat at $T = 300$ K and a Parrinello-Rahman barostat at 1 bar as reference pressure. All the dynamics were run using periodic boundary conditions and a cutoff of 1 nm for the short range forces.

For the Potential of Mean Force (PMF) calculations we used Umbrella Sampling at increasing plate distances in intervals of 0.03 nm. Every Umbrella window was first equilibrated for 2 ns and the data were collected for 4 additional nanoseconds. The restraining bias potential was set differently for every system according to the energy required to overcome the respective dehydration energy barrier (they are carefully selected by a trial and error process and obviously differ between charged and non-charged systems). We used the weighted histogram analysis method (WHAM) [34] to obtain the PMF from the collected data. Finally we performed PMF calculations for neutral plates of chemical environments identical to the charged ones for comparison purposes. We used the trajectories obtained during the Umbrella Sampling method to conduct additional analysis of the water behavior over the approaching plates.

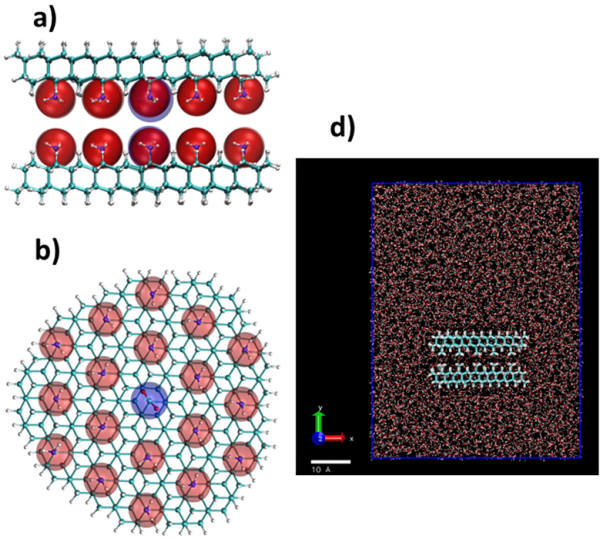

c)

System	Charged groups (blue sphere)	Chemical environment (red spheres)
S1	NH_3^+ / CO_2^- (center)	none
S2	NH_3^+ / CO_2^- (center)	NH_2 (hydrophilic)
S3	NH_3^+ / CO_2^- (center)	CH_3 / NH_2 (mixed)
S4	NH_3^+ / CO_2^- (center)	CH_3 (hydrophobic)
S5	NH_3^+ / CO_2^- (center)	CH_3 ($\varepsilon_{LJ}/2$) (more hydrophobic)

Fig. 1. (a) Side view representation of simulated parallel plates. (b) Top view of one of the parallel plates. Each plate consists of a diamond slab (grey atoms), with central opposing charged groups (blue sphere) and different chemical environments (red spheres). For the charged groups the charge is distributed between the different constituent atoms. (c) Functional groups in the simulated parallel plates as represented in (b). In S5 the Lennard-Jones parameters of the carbon atoms are reduced (to half their value) in order to yield a more hydrophobic behavior. (d) We also include a snapshot of the simulation box for one of the cases under study in order to better illustrate the simulation conditions.

We also performed a solvation thermodynamic mapping study of the molecular surface of the systems of interest by means of the Grid Inhomogeneous Solvation Theory (GIST) method, recently included [35–37] in AmberTools [38]. We used the TIP3P water model. The simulations used a periodic box (at least 15 Å between any heavy atom of the system and the edge of the periodic box). Energy minimization, followed by MD simulation, was carried out with the Amber 12 software. First, the energy of the system was minimized in two rounds; both used 1500 steps of the steepest descents algorithm followed by the conjugate gradient method for a maximum of 2000 steps. In the first round, all atoms were harmonically restrained to their initial positions with a force constant of 100 kcal/mol/Å^2. In the second round, the system was further relaxed keeping only non-hydrogen atoms restrained, with the same force constant. The energy minimized system was then heated with a series of 20 ps constant volume and temperature MD simulations with the first simulation at 50 K and incremented by 50 K every 20 ps until 300 K was reached.

The system was then equilibrated for 10 ns at 300 K at a constant pressure of 1 atm. At the final volume, the system was then equilibrated for an additional 5 ns at constant volume. The final MD production run of 20 ns was at constant number of particles, volume, and temperature (NVT) and system configurations were stored every 1 ps for a total of 20000 configurations. During all MD simulations, all atoms were harmonically restrained to their positions following the energy minimization step, with a force constant of 100 kcal/mol/Å^2. The SHAKE algorithm was used to constrain the lengths of all bonds involving hydrogen atoms. Temperature was regulated by Langevin dynamics with a collision frequency of 2.0 ps^{-1}. A 9 Å cutoff was applied to all non-bonded interactions. The main GIST solvation maps were produced from these configurations.

3 Results

In order to achieve the goals proposed for this work, a detailed and systematic exploration of relevant combinations of charge and surroundings must be conducted for the systems under study. For sake of clarity we will start presenting the overall binding-energy differences between the different charged plates to single out the relevance of the solvent effect. Relevant comparisons with the corresponding versions of uncharged plates will be also established.

3.1 PMF studies of charged plates

Figure 2 displays the potential of mean force (PMF) for two parallel charged plates with different chemical environments as a function of the interplate distance. The binding energy obtained for each system is the difference in energy between the global minima (at low separation) and the plateau level. From the PMF in water a clear tendency is evident: as the hydrophobicity of the groups surrounding the charge increases, the absolute value of the binding energy increases. Additionally, the position and sizes of the secondary peaks and valleys gives us information about the different stages of the dehydration process for each system. Even more, the last shoulder in the energy landscape before dehydration (the shoulder that occurs at separations a bit larger than the global minimum) provides the precise distance at which the final layer of water is removed. The PMFs in vacuum do not show significant differences.

In agreement with the binding-energy tendency, the distance at which dehydration (dewetting) of the plates occurs progressively increases as the plate becomes more hydrophobic (such distance is marked by the position of the last shoulder in the PMF). This fact will be corroborated later on with a study of the water density in the interplate region. Thus, charged hydrophobic plates induce dewetting (drying) at non-trivial distances (plate-plate separations larger than a regular water hydration layer; namely at around 5–6 Å, a distance that would accomodate a layer of water molecules), while the collapse of charged hydrophilic plates is possible only when the last

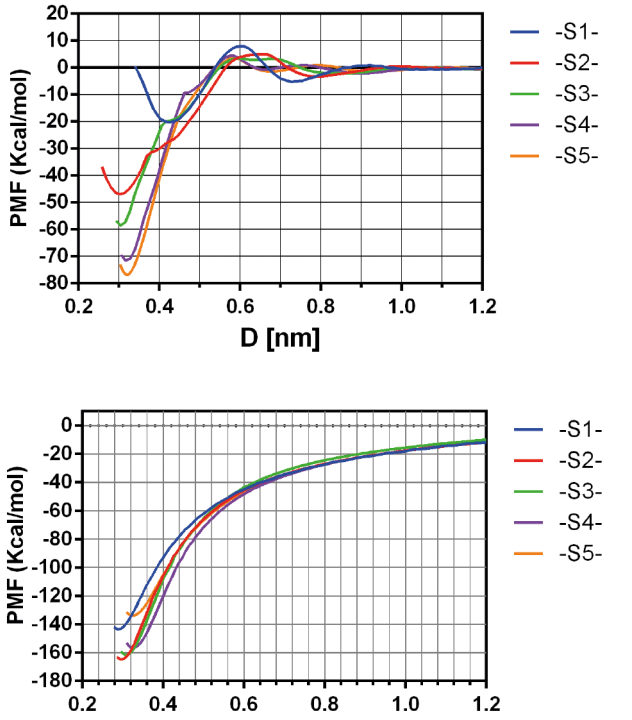

Fig. 2. Potential of mean force for the different simulated systems (listed in fig. 1(c)) as a function of the plate distance (the distances are measured between the positions of the charged groups of both plates). Top: In water PMF, Bottom: In vacuum.

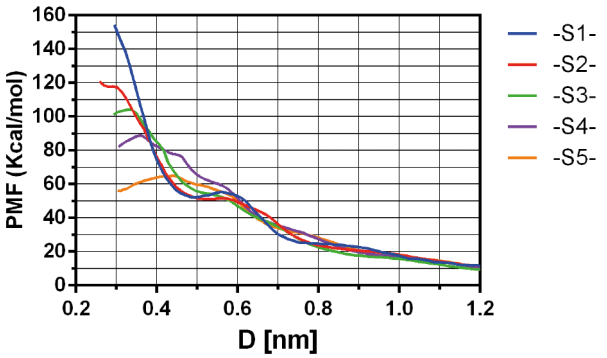

Fig. 3. Water induced potential of mean force as a function of the plate distance for different environments. Simulated systems as listed in fig. 1(c).

water layer is finally expelled by steric effects. A minor observation worth mentioning is the special case of system S1, in which no functional groups surround the charge (the charged group protrudes) and, thus, such liberated space is occupied for an extra layer of water. In this situation, the minimum of the Potential of mean force appears at a greater distance than the others due to the impossibility for the steric displacement of such last layer of water.

In order to single out the effect of water on the self-assembly process, we show in fig. 3 the water-induced potential of mean force for the same systems discussed above. This graph was obtained by subtracting point by point the PMF in vacuum from the corresponding PMF

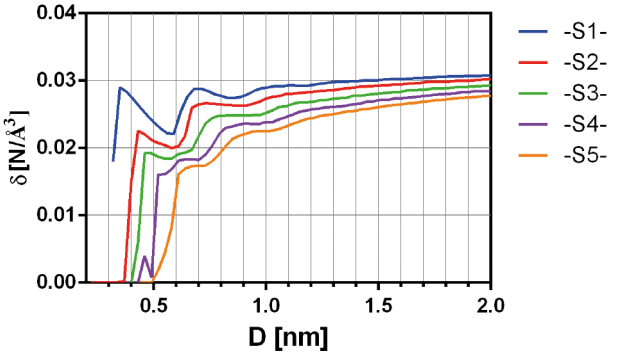

Fig. 4. Water molecular density between plates as a function of distance for the systems listed in fig. 1(c).

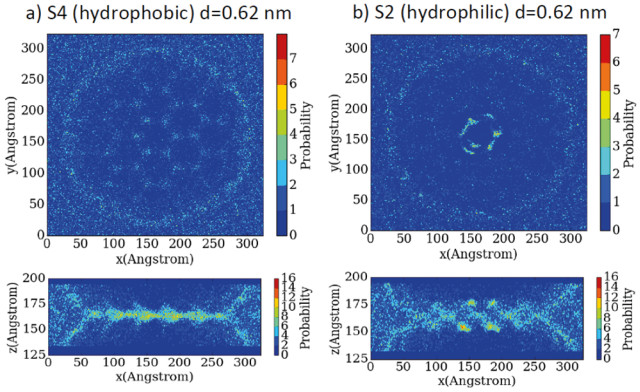

Fig. 5. Heat map of the 2D molecular density for (a) system S4 (hydrophobic environment) at 0.62 nm of distance between plates; (b) system S2 (hydrophilic environment) at 0.62 nm of distance between plates. Top panels represents top view and lower panels the lateral view. The color scale represents the number of water molecules.

in water (as shown in fig. 2). Since all the in vacuo PMF are very similar (with a maximum difference of about 12 per cent), we can conclude that the differences in binding energies seen in fig. 2 arise as a consequence of the different behavior of hydration water on each system. It is not trivial to mention that in all the cases presented so far the net effect of water is always repulsive (*i.e.* hydrophilic like, as a consequence of the charges), being less repulsive as the chemical character of the neighboring groups become more hydrophobic. The situation is different for the non-charged plates. Later on we will discuss this difference in order to single out the context-dependent effect of the charges and where we shall deal with both overall hydrophobic and hydrophilic systems. However, before proceeding to the analysis of the neutral versions of the plates, we will present some additional examination of water as the charged slabs approach each other. All these calculations were made over the equilibrated trajectories of each umbrella sampling window.

In fig. 4 we depict the water molecular density profile as a function of the distance between the plates (calculated as the average water density in the entire space between the diamond slabs, over all the time span of every umbrella window). As above-mentioned, the density drops earlier as the groups surrounding the charge become more hydrophobic. This is in concordance with the argued dewetting transition observed in the PMF (fig. 2). More hydrophobic plates have a dewetting transition at larger plate separation.

It is interesting to also analyze the local distribution of water density in between the plates. In fig. 5 we show the 2D spatial density distribution at a selected distance (0.62 nm) between two different charged-plates cases: S2 (hydrophilic environment) and S4 (hydrophobic). Both the lateral and the top profile views give us an idea of the influence of the local surrounding context on the charged region. The hydrophobic methyl groups clearly promote the dehydration of the charged moiety under nano-confinement, while the charge surrounded by the polar NH2 groups remains tightly hydrated at such plate-plate separation. It is interesting to note that in both cases we can observe a slightly high water density near the borders of the plates. Moreover in the case of the hydrophobic environment (fig. 5(a)) we can observe an ordering motif similar to the diamond structure of the plates, suggesting that the hydrophobic characteristic of the plates is not that strong.

3.2 PMF studies of neutral plates

For comparison, we generated a series of neutral plates by removing the charged functional group from the plates previously studied. In fig. 6 we depict the neutral systems and the corresponding simulated environments.

For such systems we performed the corresponding PMF calculations. We can observe in the PMF in water of fig. 7 that the removal of the charges from the plates makes the previously observed binding-energy differences almost disappear. Perhaps the most intriguing observation is the favorable energy of binding for the system S2′ (hydrophilic), but this may be due to the contribution of a number of minor effects: for instance, the hydrophobic driven collapse depends on the whole volume of the plate, and not only on the chemical identity of the functionalized face; also, the NH_2 groups face allows for a certain degree of electrostatic interaction once the water in between the plates is expelled. It is also worth noticing that the peaks and valleys obtained for the neutral plates match almost perfectly the distances observed in their charged equivalents (fig. 2), thus indicating that the behavior of the solvent at the interface is primarily determined by the collective chemical nature of the plate and is not significantly altered by the central charge.

We next studied the effect of water on the uncharged systems. Even when a full description of the process of assembling of the neutral systems is not intended in this work, a better understanding of these systems may shed some light on the comprehension of the dependence of the behavior of nano-confined water the on the chemical nature of the interface. As shown in fig. 8, except for the Lennard-Jones modified slab which exhibits a neat

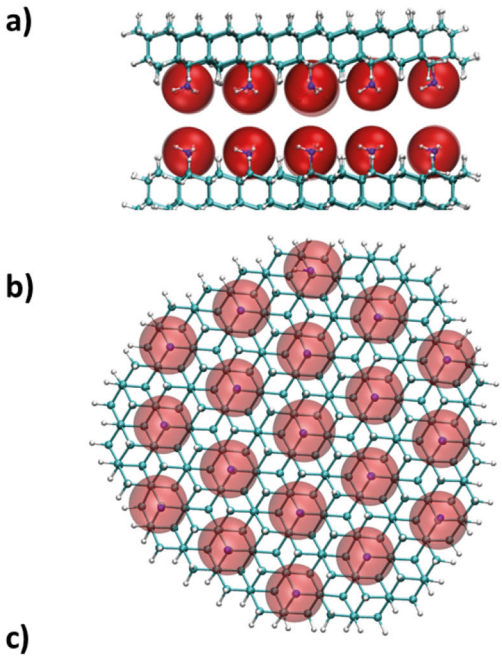

System	Charged groups	Chemical environment (red spheres)
S2′	none	NH_2 (hydrophilic)
S3′	none	CH_3 / NH_2 (mixed)
S4′	none	CH_3 (hydrophobic)
S5′	none	CH_3 ($\epsilon_{LJ}/2$) (more hydrophobic)

Fig. 6. (a) Side view representation of simulated parallel plates. (b) Top view of one of the parallel plates. Each plate consists of a diamond slab (grey atoms) and different chemical environments (red spheres). (c) Functional groups in the simulated parallel plates as represented in (b). The systems employed represent the uncharged counterparts of the ones shown in fig. 1. To emphasize such correspondence, we have labeled them as S2′ (the uncharged system to compare with S2), S3′ (the uncharged system to compare with S3) and so on. Thus, S2′ means that in each of the two parallel plates we have removed the central charged group (in the table we indicate by "none" the number of charged groups) and replaced it by a group of the correponding environment kind, in this case a hydrophilic group (in such way, the plates now contain all red spheres, in this case hydrophilic groups).

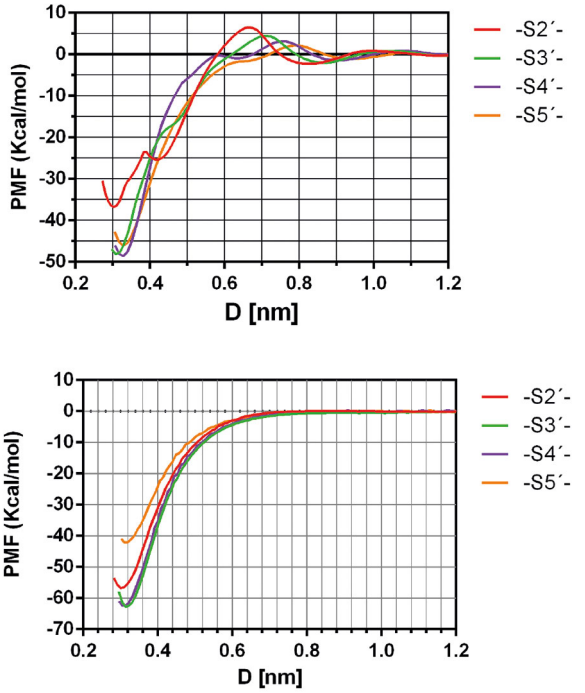

Fig. 7. Potential of mean force for the different simulated systems (listed in fig. 6(c)) as a function of the plate distance. TOP: PMF in water. Bottom: In vacuum.

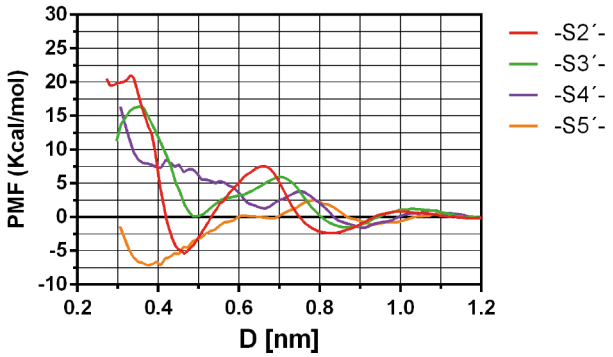

Fig. 8. Water induced potential of mean force as a function of the plate distance for different environments. Simulated systems as listed in fig. 6(c).

hydrophobic behavior, the water effect is always repulsive. Previous results on graphene-like systems [9, 39–44] (whose behavior has been demonstrated to be rather hydrophilic both in simulations and experimental studies) suggest that this effect may be due by the very dense packing of carbon atoms in the backbone of the present diamond-like model. In fact, the Van der Waals terms acting over the plates could be large enough to compete with the water-water interaction efficiently [9, 39–44] (see also fig. 5). This is, in fact, the reason for our decision to include a model with C-C reduced interactions ($\epsilon_{LJ}/2$) in this study, a strategy that has also been already used in graphitic contexts [9, 44], to satisfy the need to consider the effect of a proper hydrophobic background.

3.3 Direct comparison of neutral and charged systems

In order to single out the context-dependent contribution of the electrostatic interaction to the binding of the plates, we show in fig. 9 the result of subtracting the energy landscape obtained in water for neutral systems from their charged relatives. As directly evident from the figure, there is a remarkable variation on the energy change resultant from considering the exact same charge within different chemical environments. In fact, the two contexts that represent extremes in chemical dissimilarity present a difference of roughly 20 kcal/mol.

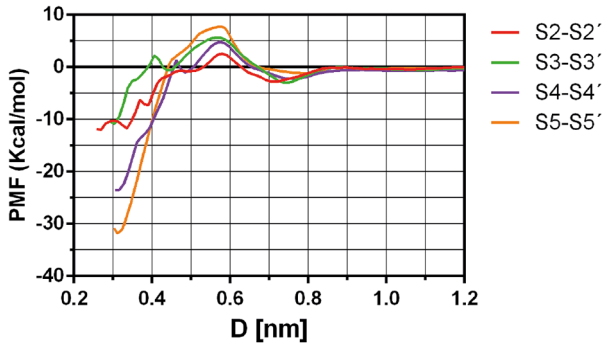

Fig. 9. Potential of mean force, in water, resulting from the difference between neutral and charged systems. PMF is displayed as a function of the plate distance for different environments. Simulated systems as listed in fig. 6(c) and fig. 1(c). S2 - S2′ means that we are subtracting the PMF for the uncharged S2′ system from the one of the charged S2 system, S3 - S3′ implies the difference between the PMFs of S3 and S3′, and so on.

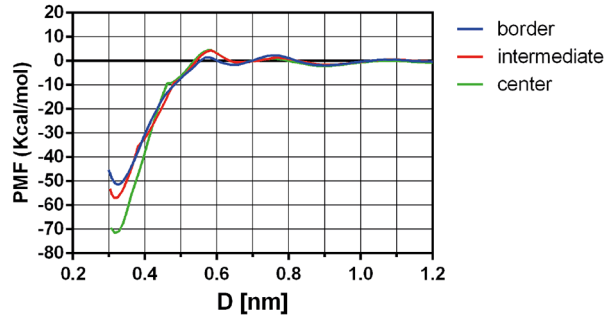

Fig. 10. Potential of mean force for the charged hydrophobic system (similar to S4 in fig. 2), with the charged group located at different positions in the plates.

3.4 Study of single charges at different locations

To further inspect the context-dependent nature of the electrostatic interactions, we now consider the same background system, hydrophobically functionalized plates made of diamond-like slabs ending with CH_3 groups, where a charged group replaces one CH_3 at different locations of the slab: at the center of the plates (same system as S4 in fig. 2), at the border and at an intermediate location between the center and the border of the plate. In each case, the other slab is identical, but with an oppositely charged group. Thus, the three cases under study are chemically identical (equal composition of charged and hydrophobic sites), except for the fact that the charges are located at different positions within the interface and thus, any difference in their behavior would be due to their locally different environments. Figure 10 shows the results. The value of the minimum for the case of the charge located at the center of the slabs is more pronounced than for the border case (the intermediate charge location presents an intermediate behavior, closer to the behavior for the centre charge). It is evident that upon self-assembly, charges at the centre of the interface are properly protected from the effect of water by the surrounding hydrophobic groups, while for charges at the border this requisite would not be completely satisfied. Charges at an intermediate location are nonetheless surrounded by hydrophobes and thus they are fairly well shielded from water. It is notable that in proteins hot spots are indeed generally located at the center of the protein interface where they can be well protected from the solvent [30,31].

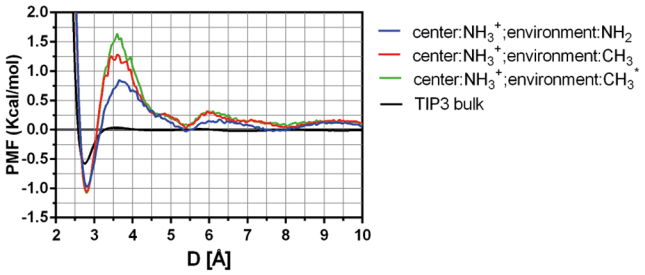

Fig. 11. Potential of mean force based on the water-water radial distribution function for isolated plates.

3.5 Isolated plates analysis

In order to gain a deeper comprehension on the behavior of water vicinal to the surfaces of the models, we also conducted a series of simulations for the corresponding isolated plates (only one plate) in water. To this end, we calculated the potential of mean force for water approaching the central charge. Such quantity was obtained by computing first the water-water radial distribution function of water molecules (along radially increasing semicircles) and then calculating the mean force profile as: $PMF(r) = -k_B T \ln g(r) + C$. A plot of this quantity is shown in fig. 11, from which we can learn that even when there is virtually no difference in the net energy of bringing a water molecule from the bulk to the proximity of the charge for the different systems, the energy required to overcome the barrier varies by about 1 kcal/mol (which is almost the total depth of the well). This fact would be meaningful if we consider that such energy cost represents the energy required to displace the water molecules surrounding the charge, especially because the easiness of water removal is very likely to be extrapolated to the situation in which, instead of another water molecule, a ligand is approaching the charge.

Finally, we also carried out GIST calculations for single plates with a central charge within three different kinds of environments of increasing hydrophobicity, that is, the hydrophilic (NH_2 terminated) plates, plates with CH_3 groups and hydrophobic plates terminated in CH_3 groups with reduced interactions (modified Lennard-Jones parameters, $\epsilon_{LJ}/2$). The results are shown in fig. 12(a). We can see that the system with a strong hydrophobic environment (CH_3 with reduced Lennard-Jones interactions) displays a higher propensity to dehydration even at regions close to the charge, while the system with the hydrophilic environment (NH_2 terminated) is the one that

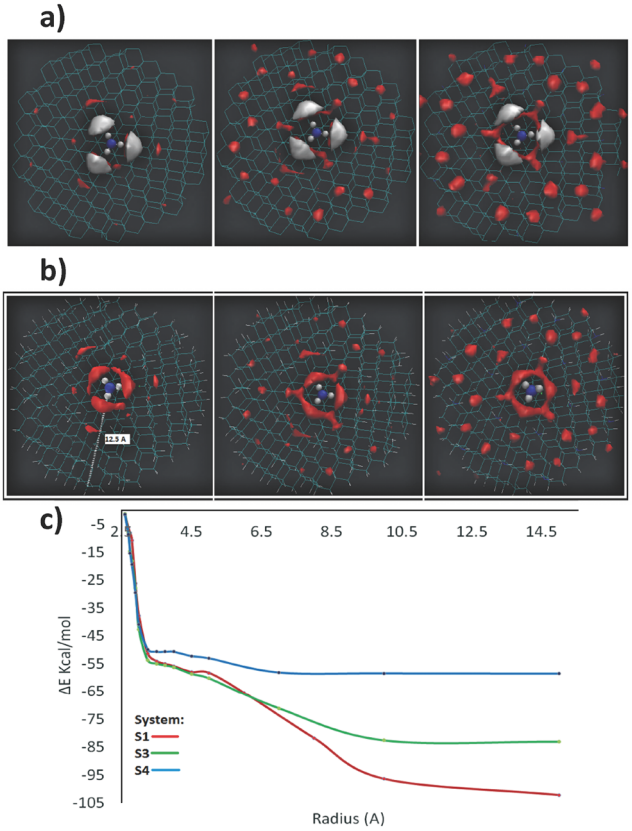

Fig. 12. (a) GIST study for: hydrophilic (left), hydrophobic (center) and more hydrophobic (interaction reduced to half its value, $\epsilon_{LJ}/2$) (right). Red color represents sites where the oxygen density is 4 times higher than the bulk water. White color represents sites where the hydrogen density is 4 times higher than the bulk water. (b) GIST study for water with interaction of at least 0.1 kcal/mol, for hydrophilic (left), hydrophobic (center) and more hydrophobic ($\epsilon_{LJ}/2$) (right). (c) Cummulative solvent interaction energy (calculated from the sum boxes with interaction energy larger than 0.1 kcal/mol) measured radially form the charge.

presents the tighter hydration (sites with water density more than four times that of the bulk). The normal CH_3 terminated plate presents an intermediate behavior but closer to the hydrophilic plate, as expected. It is interesting to note that the water molecules directly interacting with the charge are the only ones that present a clear orientational preference so that regions of hydrogen density more than four times larger than the bulk (white spots) are found only at such regions. The plots of regions of high solvent interaction energy fig. 12(b) (energies of at least 0.1 kcal/mol) indicate an enhanced solvent interaction for the hydrophilic plate as compared to the hydrophobic case, as expected. In particular, we can appreciate a very well defined ring region of tight binding around the charge. The hydrophobic plate (CH_3 with reduced Lennard-Jones interactions) displays a more desolvated context, and even a weakening of the region around the charge: the ring is not completely formed. This fact speaks of the existence of a shell of more easily removable water around the charge. Of course, given the fact that we are dealing with isolated plates, the charge always retains hydration water and the hydrophobes are only able to labilize such water very slightly. However, upon approach of another complementary charged plate with the concurrent nano-confinement, the local environment is more effective in inducing drying (as shown in our previous PMFs for pairs of parallel plates and in the corresponding water density fluctuation analysis). In fig. 12(c) we also show the results of the sum of the interaction energies of all the solvent sites (boxes with energy larger than 0.1 kcal/mol) calculated on spheres of increasing large around the positive charge. The system with an environment of Lennard-Jones reduced CH_3 groups (properly hydrophobic environment) yields a global solvent interaction energy lower in roughly 5 kcal/mol when calculated at distances commensurate with the first water hydration shell (below 4 Å). Thus, the difficulty to remove the water molecules from the first hydration shell of the charge is reduced when the charge is located within a hydrophobic environment. The figure also shows that such difference grows as the radius of the sphere is increased.

4 Conclusion

In this work we have studied PMF calculations for pairs of parallel plates in which charged functional groups interact within chemically different local environments. We have shown that by increasing the hydrophobicity of the surroundings, the interaction energy grows significantly. Additionally, from the water-induced PMFs we learn that this effect is indeed owed to the solvent behavior. Moreover, by subtracting the energy profiles obtained for neutral systems from their charged relatives we make evident the non-additive effect of the non-covalent interactions involved in the process: The electrostatic attraction is clearly enhanced by the local hydrophobic effect. Also, for systems of identical chemistry (single charged groups immersed in a sea of hydrophobic groups) we show that plate attraction clearly depends on the location of the charged group (center or border of the plates) provided the different level of protection from the solvent they attain. Finally, studying pairs of parallel charged plates (and also isolated charged plates) we show that as the local hydrophobicity increases, the dehydration propensity grows even for the water molecules in close proximity of the charged groups, thus enhancing charge attraction and promoting the self-assembly process. Our results for simple model systems give support to a scenario of protein binding in which the local hydrophobicity becomes a central ingredient for modulating electrostatic interactions upon binding. In materials science, in turn, there exist several aqueous self-assembly problems where the study of the interplay between hydrophobic and electrostatic interactions might be relevant, as for example the molecular intercalation between hydrophobic surfaces such as graphene or graphene oxide sheets (which has practical interest both for promoting graphene exfoliation or for preventing it as in lithium ion batteries electrodes) [45–47].

For example, it has been found that the differences in the aggregation rate of different graphene oxides should be attributed to the hydrogen bonds [45]. While hydrogen bonds might result irrelevant as electrostatic intermolecular interactions when water exposed, in the light of the previous discussion we can figure out their strengthening within a hydrophobic nano-confinened environment.

Financial support from CONICET, ANPCyT and UNS is gratefully acknowledged. GAA and SRA are research fellows of CONICET and JMMO and CAM thank CONICET for a fellowsip.

Author contribution statement

All authors contributed equally to this work.

References

1. D. Chandler, Nature **437**, 640 (2005).
2. G. Hummer, J.C. Rasaiah, J.P. Noworyta, Nature **414**, 188 (2001).
3. S. Vaitheeswaran, H. Yin, J.C. Rasaiah, G. Hummer, Proc. Natl. Acad. Sci. U.S.A. **101**, 17002 (2004).
4. J.C. Rasaiah, S. Garde, G. Hummer, Annu. Rev. Phys. Chem. **59**, 713 (2008).
5. G. Cicero *et al.*, J. Am. Chem. Soc. **130**, 1871 (2008).
6. N. Choudhury, B. Montgomery Pettitt, J. Phys. Chem. B **109**, 6422 (2005).
7. N. Giovambattista, P.J. Rossky, P.G. Debenedetti, Annu. Rev. Phys. Chem. **63**, 179 (2012).
8. N. Giovambattista, P.G. Debenedetti, C.F. Lopez, P.J. Rossky, Proc. Natl. Acad. Sci. U.S.A. **105**, 2274 (2008).
9. S.R. Accordino, J.M. Montes de Oca, J.A. Rodriguez Fris, G.A. Appignanesi, J. Chem. Phys. **143**, 154704 (2015).
10. N. Giovambattista, P.G. Debenedetti, P.J. Rossky, Proc. Natl. Acad. Sci. **106**, 15181 (2009).
11. B.J. Berne, J.D. Weeks, R. Zhou, Annu. Rev. Phys. Chem. **60**, 85 (2009).
12. J.L. Kulp III, J.R. Kulp Jr., D.L. Pompliano, F. Guarnieri, J. Am. Chem. Soc. **133**, 10740 (2011).
13. L.M. Alarcón, D.C. Malaspina, E.P. Schulz, M.A. Frechero, G.A. Appignanesi, Chem. Phys. **388**, 47 (2011).
14. E. Schulz, M. Frechero, G. Appignanesi, A. Fernández, PLoS ONE **5**, e12844 (2010).
15. E.P. Schulz, L.M. Alarcón, G.A. Appignanesi, Eur. Phys. J. E **34**, 114 (2011).
16. S.R. Accordino, D.C. Malaspina, J.A. Rodriguez Fris, G.A. Appignanesi, Phys. Rev. Lett. **106**, 029801 (2011).
17. K. Lum, D. Chandler, J.D. Weeks, J. Phys. Chem. B **103**, 4570 (1999).
18. D. Huan, C.J. Margulis, B.J. Berne, Proc. Natl. Acad. Sci. U.S.A. **100**, 11953 (2003).
19. L. Hua, R. Zangi, B.J. Berne, J. Chem. Phys. C **113**, 5244 (2009).
20. H. Acharya, S. Vembanur, S.N. Jamadagni, S. Garde, Faraday Discuss. **146**, 353 (2010).
21. S.N. Jamadagni, R. Godawat, S. Garde, Annu. Rev. Chem. Biomol. Eng. **2**, 147 (2011).
22. A. Fernández, in *Transformative Concepts for Drug Design: Target Wrapping*, Vol. **1** (Springer, Heidelberg, 2010) pp. 1–224.
23. A. Fernández, R. Scott, Phys. Rev. Lett. **91**, 018102 (2003).
24. S.R. Accordino, J.A. Rodriguez-Fris, G.A. Appignanesi, A. Fernández, Eur. Phys. J. E **35**, 59 (2012).
25. S.R. Accordino, M.A. Morini, M.B. Sierra, J.A. Rodriguez Fris, G.A. Appignanesi, A. Fernández, Proteins Struct. Funct. Bioinf. **80**, 1755 (2012).
26. M.B. Sierra, S.R. Accordino, J.A. Rodriguez-Fris, M.A. Morini, G.A. Appignanesi, A. Fernández Stigliano, Eur. Phys. J. E **36**, 62 (2013).
27. S.R. Accordino, J.A. Rodriguez Fris, G.A. Appignanesi, PLoS ONE **8**, e55123 (2013).
28. C.A. Menéndez, S.R. Accordino, D.C. Gerbino, G.A. Appignanesi, Eur. Phys. J. E **38**, 107 (2015).
29. C.A. Menéndez, S.R. Accordino, D.C. Gerbino, G.A. Appignanesi, PLoS ONE **11**, e0165767 (2016).
30. A.A. Bogan, K.S. Thorn, J. Mol. Biol. **208**, 1 (1998).
31. J. Li, Q. Liu, Bioinformatics **25**, 743 (2009).
32. H.J.C. Berendsen, D. van der Spoel, R. van Drunen, Comput. Phys. Commun. **91**, 43 (1995).
33. J. Wang, W. Wang, P.A. Kollman, D.A. Case, J. Mol. Graph. Mod. **25**, 247260 (2006).
34. S. Kumar, J.M. Rosenberg, D. Bouzida, R.H. Swendsen, P.A. Kollman, J. Comput. Chem. **13**, 1011 (1992).
35. S. Ramsey, C. Nguyen, R. Salomon-Ferrer, R.C. Walker, M.K. Gilson, T. Kurtzman, J. Comput. Chem. **37**, 2029 (2016).
36. C.N. Nguyen, M.K. Gilson, T. Young, arXiv:1108.4876 (2011).
37. C.N. Nguyen, A. Cruz, M.K. Gilson, T. Kurtzman, J. Chem. Theor. Comput. **10**, 2769 (2014).
38. D.A. Case *et al.*, *AMBER 10* (University of California, San Francisco, 2008).
39. Z. Li *et al.*, Nat. Mater. **12**, 925 (2013).
40. L. Li, D. Bedrov, G.D. Smith, J. Chem. Phys. **123**, 204504 (2005).
41. L. Li, D. Bedrov, G.D. Smith, J. Phys. Chem. B **110**, 10509 (2006).
42. M.V. Athawale, S.N. Jamadagni, S. Garde, J. Chem. Phys. **131**, 115102 (2009).
43. Chih-Jen Shih, S. Lin, M.S. Strano, D. Blankschtein, J. Am. Chem. Soc. **132**, 14638 (2010).
44. G. Hummer, J.C. Rasaiah, J.P. Noworyta, Nature **414**, 188 (2001).
45. H. Tang, D. Liu, Y. Zhao, X. Yang, J. Lu, F. Cui, J. Phys. Chem. C **119**, 26712 (2015).
46. O.-S. Lee, M. Carignano, J. Phys. Chem. C **119**, 19415 (2015).
47. V.V. Chaban, E.E. Fileti, O.V. Prezhdo, J. Phys. Chem. C **121**, 911 (2017).